COMMISSARIAT À L'ÉNERGIE ATOMIQUE

DSM - DAPNIA

DIRECTION DES SCIENCES DE LA MATIÈRE

DEPARTEMENT D'ASTROPHYSIQUE, DE PHYSIQUE DES PARTICULES,
DE PHYSIQUE NUCLÉAIRE ET DE L'INSTRUMENTATION ASSOCIÉE

SERVICE D'ÉTUDE DES ACCÉLÉRATEURS

Nicolas PICHOFF

NOTE	
DATE : 11/09/98 N/RÉF. : DAPNIA/SEA 98/45	OBJET : Halo from Coulomb Scattering of Beam Particles on Residual Gas V/RÉF. :
DE : Nicolas PICHOFF	A : Jean-Michel LAGNIEL

HALO FROM COULOMB SCATTERING OF BEAM PARTICLES ON RESIDUAL GAS

Nicolas PICHOFF, Pierre-Yves BEAUVAIS
Commissariat à l'Energie Atomique - DSM/DAPNIA/SEA
91191 Gif-sur-Yvette cedex. FRANCE.

Gérard HAOUAT
Commissariat à l'Energie Atomique - Direction des Applications Militaires
BP12 91680 Bruyères-le-Châtel. FRANCE.

Abstract

The contribution of coulomb elastic scattering of beam particles on the residual gas to the beam halo development in a linear accelerator is studied. Starting from the basic differential cross section formula giving the probability of a particle to scatter at a given angle, we analyse the behaviour of those few particles which scatter at rather large angles and we estimate their proportion relative to the beam intensity. We present a transport code dedicated to the scattering of a beam on the residual gas, which we validate with an experiment in which the beam is transported in a drift space. We use then our code to simulate the transport of a beam matched to a uniform focusing channel and we show how the collisional halo develops. The code is finally used in order to establish the loss rate per meter in a high intensity linac. This loss rate is compared to the acceptable one.

Contents

1. Introduction

The requirements of very high current linear electron and proton accelerators have increased considerably over the recent years. Beam losses are a main concern in the design of such machines. Experimental observations and theoretical predictions have shown the existence of a low-density halo surrounding the central core of a high-intensity beam. This halo not only leads to particle loss along the accelerator, but also can induce enough activity in the structures to complicate the maintenance of the machine. There are many contributions to the formation of the halo. Several theoretical studies have been undertaken recently to understand the formation of the halo through the dynamics of particle-beam transport [1][2]. However, up to now, very few attempts have been made to study halo formation via interactions of beam particles with the residual gasses of the accelerator.

The scattering of particles in the residual gas of a circular accelerator is known to be crucial for the lifetime of the beam. It is essentially due to the billion kilometres covered by the beam before its extinction. However, in a linear accelerator, the distance is not so large, and it often seems reasonable to neglect the scattering effect on the residual gas. Moreover, in a linear accelerator, the vacuum quality is not as good as in a circular one, especially near the source where the beam energy is rather low, and the scattering effects can be important. This is why some physicists have studied the influence of scattering on the beam emittance growth, and have shown that its contribution is sometimes non-negligible [3]. They have used, in their studies, a statistical description of the scattering process (including multi-scattering), thereby neglecting the detailed effect of individual scattered particles on the beam profile.

We have undertaken an experimental study of halo formation and development around an intense (50 mA), low-energy (500 keV), low-emittance (0.6 π.mm.mrad, normalized) proton beam during its transport through a periodically focusing FODO channel [4]. The aim of this study is to understand the dynamics of an intense charged particle beam submitted to the interplay of internal, repulsive, space charge forces and externally applied focusing forces [5]. In order to provide a coherent interpretation of this halo-producing process, it appears necessary to estimate the amount of halo produced by the scattering of beam particles on the residual gas, and to subtract it from the measured data.

Analysing the basic scattering process, we show that its effect is not negligible in the case of our experiment. Then, we validate a simple theoretical and numerical model by an experiment which consists in measuring over a large dynamic range the transverse profile of a proton beam at the end of a drift space, for various gas pressures. Using this model, we simulate the transport of the proton beam under our FODO experimental conditions and estimate the magnitude of the scattering-induced halo.

2. The scattering process of a proton beam

2.1. The basic process

We consider, here, the elastic Coulomb scattering of beam particles on the atoms of the residual gas in an accelerator. The probability of collisions is governed by the well known Rutherford differential cross section formula [6] :

$$\frac{d\sigma}{d\theta} = \frac{3.256\ z^2 Z^2}{E^2} \cdot \frac{1}{\sin^3\theta} \cdot \frac{(M\cos\theta + \sqrt{M^2 - m^2\sin^2\theta})^2}{M\sqrt{M^2 - m^2\sin^2\theta}} \cdot 10^{-26} \qquad \textbf{(1)}$$

where : σ is the scattering cross section (in cm^2),
θ is the scattering angle from the incident direction (in rad),
z is the incident particle charge number,
Z is the target nucleus charge number,
m is the incident particle mass,
M is the target nucleus mass,
E is the incident particle energy (in MeV).

This formula calls for three comments :

i) - The scattering cross section decreases rapidly with angle (in θ^{-3}), which means that the scattering process has no significant influence on the beam emittance growth [3]. However, the decreasing rate is much smaller than for an exponential or a Gaussian shape, which is usually used to describe a beam transverse profile. This implies that, from the halo point of view, a non-negligible number of particles can be scattered at angles greater than the mean angular dispersion of the beam. These particles, under the influence of the beam transport laws, may be rapidly kicked out into the halo region and contribute to beam losses.

ii) - Since the cross section varies as E^{-2}, the scattering process is very important for low-energy particles, which is the case in our experiment.

iii) - In most practical applications, the correction term (containing m and M) in formula **(1)** is considered as constant and equal to 4. This is justified because, on the one hand, we are dealing with small scattering angles (<100 mrad), on the other hand, the mass of the incident particle is lower than that of the target nucleus. For example, with m=1, M=16 (proton scattering on an oxygen atom), and for a scattering angle of 100 mrad, the correction term is equal to 3.98 (compared to 4 when $\theta \to 0$ and $M/m \to \infty$). So, for small angle scattering, we can use the simplified differential cross section formula :

$$\frac{d\sigma}{d\theta} = \frac{13\ z^2 Z^2}{E^2} \cdot \frac{1}{\theta^3} \cdot 10^{-26} \qquad \textbf{(2)}$$

2.2. Application to a proton beam

2.2.1. Scattering angle

Let P be the residual gas pressure (in Pascal) in the accelerator vacuum system. Using the perfect gas formula, the number of particles n (m^{-3}) per unit volume is : $n = \frac{N_A P}{RT}$ where N_A=6.02 10^{23} mol^{-1}, is Avogadro's number, R=8.315 J/mol/K is the perfect gas constant and T is the gas absolute temperature in Kelvin.

The probability per meter (m^{-1}) for a particle to scatter in one shot at an angle between θ and θ+dθ is :

$$dP(\theta) = d\sigma(\theta) \cdot n \qquad \textbf{(3)}$$

This gives for protons (z=1) in a gas at temperature T=300K:

$$dP(\theta) = \frac{0.31\, Z^2 P}{E^2} \cdot \frac{d\theta}{\theta^3} \qquad \textbf{(4)}$$

with P in hPa, E in MeV, θ and dθ in mrad.

One can notice that, according to equation **(4)**, the probability to scatter at an infinitely small angle is infinitely large, which is not physically realistic. In fact, this formula applies only for angles between a minimum angle θ_{min}, corresponding to a large impact parameter of the order of the atom radius (field screening of nucleus by electrons), and a maximum angle θ_{max}, corresponding to a small impact parameter of the order of the nucleus radius (charge distribution in the nucleus).

We have [7] : $\theta_{min} = \frac{\hbar}{pa}$ and $\theta_{max} = \frac{\hbar}{pR}$, where $\hbar$ is Planck's constant, p is the incident particle momentum, $a=1.4a_0Z^{-1/3}$m is the atom radius, with a_0=0.529 10^{-10}m the Bohr radius and $R=1.4A^{1/3}$ 10^{-15}m is the nucleus radius. **Table 1** gives the values of these extreme angles for protons of different energies, incident on nitrogen nuclei (Z=7, A=14).

Energy (keV)	**p (MeV/c)**	θ_{min} **(μrad)**	θ_{max} **(rad)**
10^1	4.33	1180	π
10^2	13.7	372	π
10^3	43.3	118	1.35
10^4	137	37	0.43
10^5	445	11.5	0.13
10^6	1670	3.0	0.034

Table 1 : Scattering limit angles for protons on oxygen

From equation **(4)**, we calculate the probability, per meter, for a particle to be scattered in one shot at an angle larger than θ_0 ($\theta_{min} < \theta_0 < \theta_{max}$) :

$$P(\theta \geq \theta_0) = \int_{\theta_0}^{\theta_{max}} dP(\theta) = \frac{0.155\, Z^2 P}{E^2} \cdot \left[\frac{1}{\theta_0^2} - \frac{1}{\theta_{max}^2} \right] \qquad (5)$$

In the case where $\theta_{max}^2 >> \theta_0^2$, we have :

$$P(\theta \geq \theta_0) = \frac{0.155\, Z^2 P}{E^2} \cdot \frac{1}{\theta_0^2} \qquad (6)$$

2.2.2. The transverse phase space

We examine now the effect of collisions with the residual gas on the transverse profile of a proton beam. In this section, the beam is assumed to have zero emittance, i.e. all proton trajectories are parallel to the propagation axis Oz, as shown in **Fig.1a**. The beam transverse profile is further observed through its projection on a given axis, say the horizontal axis Ox (**Fig.1b**).

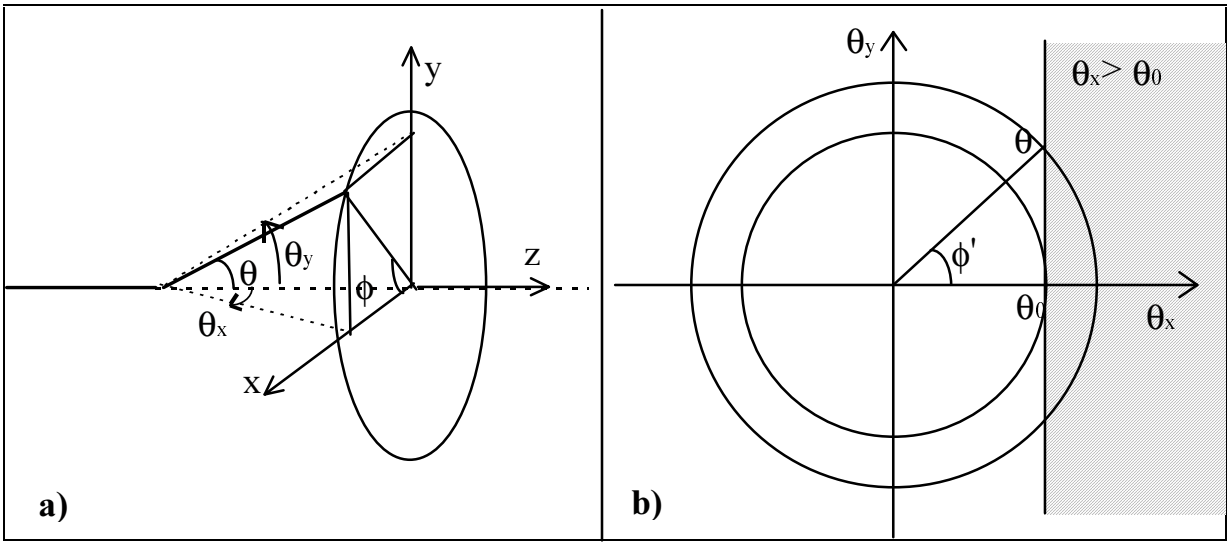

Fig. 1 : **Projection of the scattered particle trajectory on the horizontal plane.**
a) Spatial view : the particle scatters at an azimuthal angle θ and a radial angle ϕ, which gives an angle θ_x in the horizontal plane and an angle θ_y in the vertical plane.
b) Projection in the transverse space : the probability for θ_x to be greater than θ_0 is represented by the hatched part of the figure.

We consider a particular proton which is scattered in direction θ, the azimuthal angle ($\theta \in [0,\pi]$), and ϕ, the radial angle ($\phi \in [-\pi,\pi]$), with a probability $P(\theta,\phi) = P1(\theta).P2(\phi)$, since θ

and ϕ are independent variables. P1(θ) is given by expression **(4)**, P2(ϕ) is constant within [$-\pi,\pi$]. The angle of the proton trajectory, projected onto the horizontal plane xOz is θ_x. We can easily see from **Fig.1b**, that $\theta_x = \theta \cos(\phi)$. The particles scattered at an angle $\theta_x \geq \theta_0$ (hatched part of **Fig.1b**) are those scattered at an azimuthal angle $\theta \geq \theta_0$ with a radial angle ϕ such that $\cos(\phi) \leq \theta_0/\theta$, which means that $-\phi' \leq \phi \leq \phi'$ with $\cos(\phi') = \theta_0/\theta$.

We obtain :

$$P(\theta_x > \theta_0) = \int_{\max(\theta_0,\theta_{min})}^{\theta_{max}} \frac{\phi'}{\pi} \cdot \frac{dP(\theta)}{d\theta} d\theta \qquad \textbf{(7)}$$

where $\frac{\phi'}{\pi} = \frac{1}{\pi}\arccos\left(\frac{\theta_0}{\theta}\right)$ is the normalized probability for having $\theta_x \geq \theta_0$ for a given θ.

Putting $a=\theta_0/\theta$, we have :

$$P(\theta_x > \theta_0) = \frac{0.31\ Z^2 P}{E^2\theta_0^2} \int_{\theta_0/\theta_{max}}^{\min(1,\theta_0/\theta_{min})} \frac{a}{\pi} \cdot \arccos(a) da \qquad \textbf{(8)}$$

We define G(u) as :

$$G(u) = 8\int_0^u \frac{x}{\pi} \cdot \arccos(x) dx = \frac{2}{\pi}[-u\sqrt{1-u^2} + 2u^2 \arccos(u) + \arcsin(u)] \qquad \textbf{(9)}$$

we have :

G(1)=1 and G(0)=0

We finally obtain for the probability law :

$$\boxed{P(\theta_x > \theta_0) = \frac{3.9\ 10^{-2} Z^2 P}{E^2\theta_0^2} \cdot k(\theta_0)} \qquad \textbf{(10)}$$

$$\text{with } k(\theta_0) = \begin{cases} G\left(\frac{\theta_0}{\theta_{min}}\right) - G\left(\frac{\theta_0}{\theta_{max}}\right) & \text{if } \theta_0 < \theta_{min} \\ 1 - G\left(\frac{\theta_0}{\theta_{max}}\right) & \text{if } \theta_{min} \leq \theta_0 \leq \theta_{max} \\ 0 & \text{if } \theta_{max} < \theta_0 \end{cases} \qquad \textbf{(11)}$$

In the case often encountered where $\theta_{min} << \theta_0 << \theta_{max}$, we can use the formula :

$$P(\theta_x > \theta_0) = \frac{3.9\ 10^{-2} Z^2 P}{E^2 \theta_0^2} \qquad \textbf{(12)}$$

We have represented, in **Fig.2**, the variation of $P(\theta_x>\theta_0)$ with θ_0 for different proton energy values, in a monoatomic Nitrogen gas (Z=7) at a pressure of 10^{-6} hPa. The curves allow one to calculate the scattering-halo development in an accelerator by knowing the beam energy and the gas composition and pressure along the transport line.

The multi-scattering and the plural-scattering effects apply only for probabilities greater than 1 to 10 percent. In most cases considered here, they don't apply, and the model taking into account single scattering is sufficient [7]. But sometimes, especially for low-energy protons scattered at small angles, in a high-pressure gas over a long distance, we have to use the statistic-scattering models.

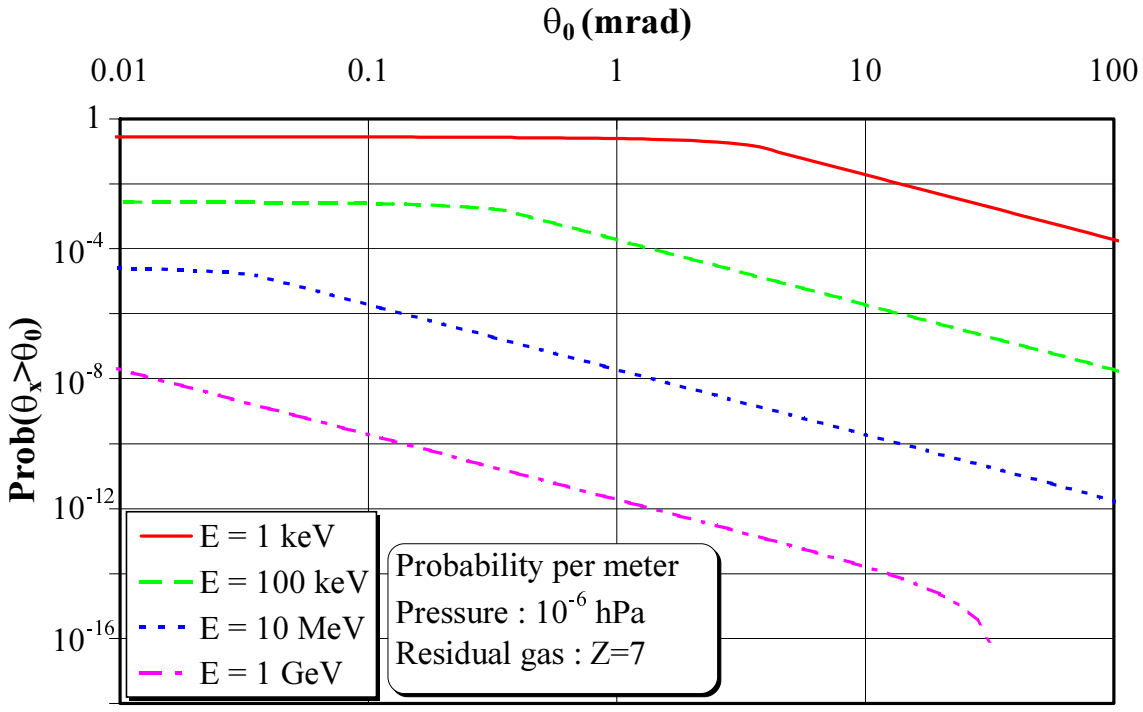

Fig. 2 : Probabilities, per meter, for protons of different energies to scatter at an angle θ_x greater than θ_0 in a monatomic Nitrogen gas at the pressure of 10^{-6} hPa.

2.2.3 Beam with small angular spread

In the preceding calculation, we have assumed a beam without angular spread. Nevertheless, a real beam has an angular spread (even small). A particle trajectory make an initial non zero slope x'_i with the beam propagation axe.

Assuming $x'_i << 1$, and scattering x-projected angle $\theta_x << 1$, the final particle slope x_f can be written :

$$x'_f = x'_i + \theta_x \, .$$

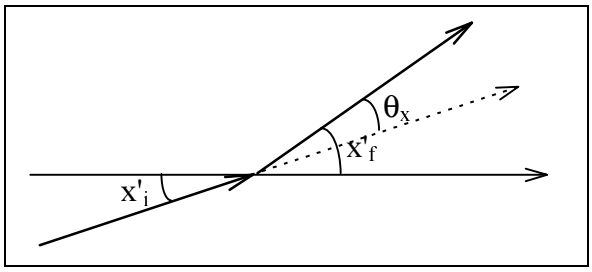

3. Experimental observation

3.1. Experimental results

The experimental set-up is schematically presented in **Fig. 3**. A 500 keV pulsed proton beam, with 500 μs pulse duration, 50 mA peak current, and 1 Hz repetition rate, is delivered by a duoplasmatron source. The beam transverse profile of a is limited by a first diaphragm (ϕ4), with 4 mm diameter, located at the exit of the source, and a second one (ϕ9), with 9 mm diameter, placed downstream 1.3 m from the first one. This diaphragms combination has been adopted to obtain a beam core with homogenous transverse profile and sharp edges, which ensures accurate observation of the collisional halo. The collimated beam propagates through a drift space toward a scintillating screen located downstream 2.8 m from the first diaphragm (ϕ4) and observed with an intensified CCD camera. This imaging technique is very powerful since it allows density distribution measurements over a very large dynamic range [8]. This scintillating screen is home made. It consists of P47 phosphor crystal powder deposited on a rectangular stainless steel plate. The gas pressure in the evacuated transport line can be changed by injecting nitrogen gas at the level of the scintillating screen. The gas pressure is measured at three locations in the transport line : at the beginning close to the source, in the middle near diaphragm ϕ9, and at the end in the vicinity of the phosphor screen.

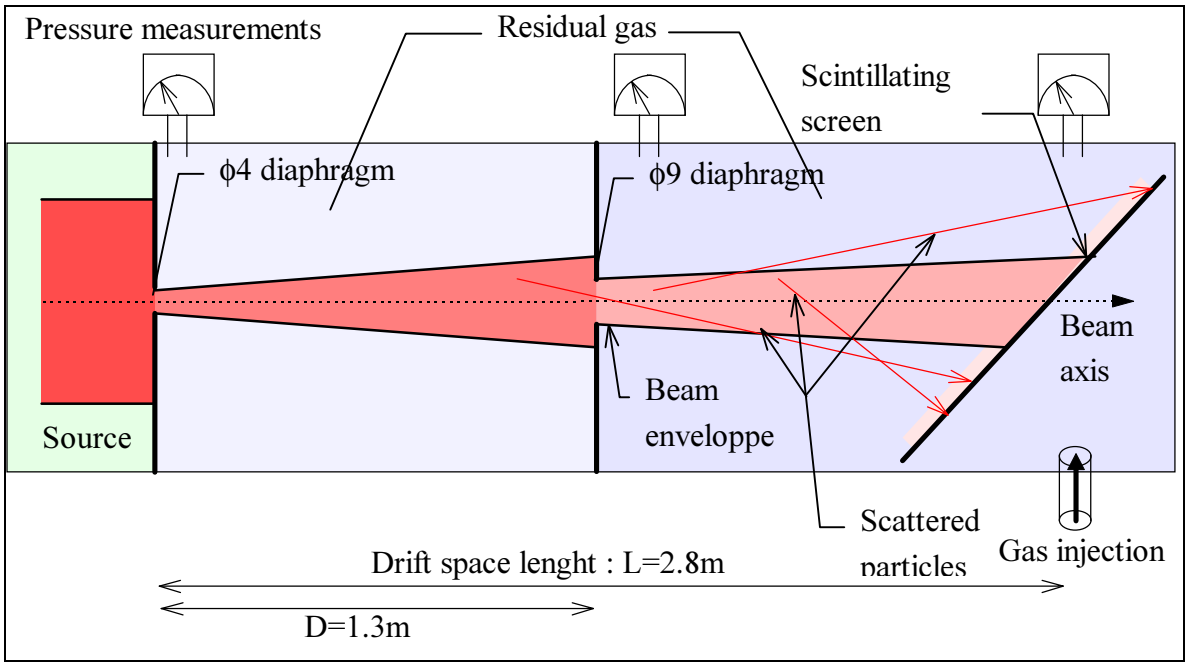

Fig. 3 : Schematic experimental set-up

The beam profile is observed on a wide dynamic range by progressively moving the phosphor screen toward the beam centre. For each screen position, the light intensification is adjusted to get an analysable image of the halo, as shown on **Fig. 4**.

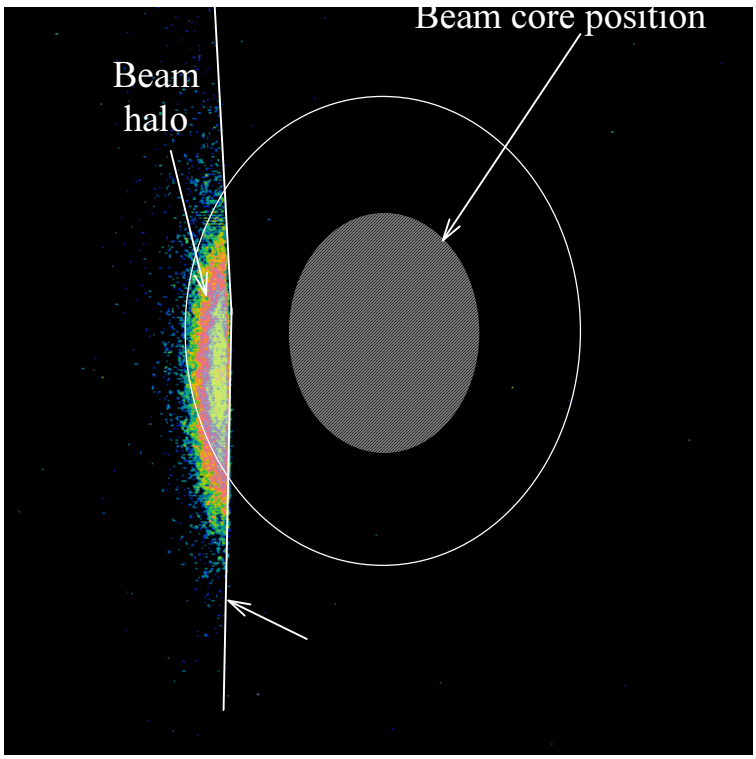

Fig. 4 : Image of the scattering halo with a scintillating screen partly on the path of the beam.

The total beam profile is, further, restored using the light intensifier calibration curve. Beam profiles are presented in **Fig. 5** for two different nitrogen-gas pressure sets given in **table 2**.

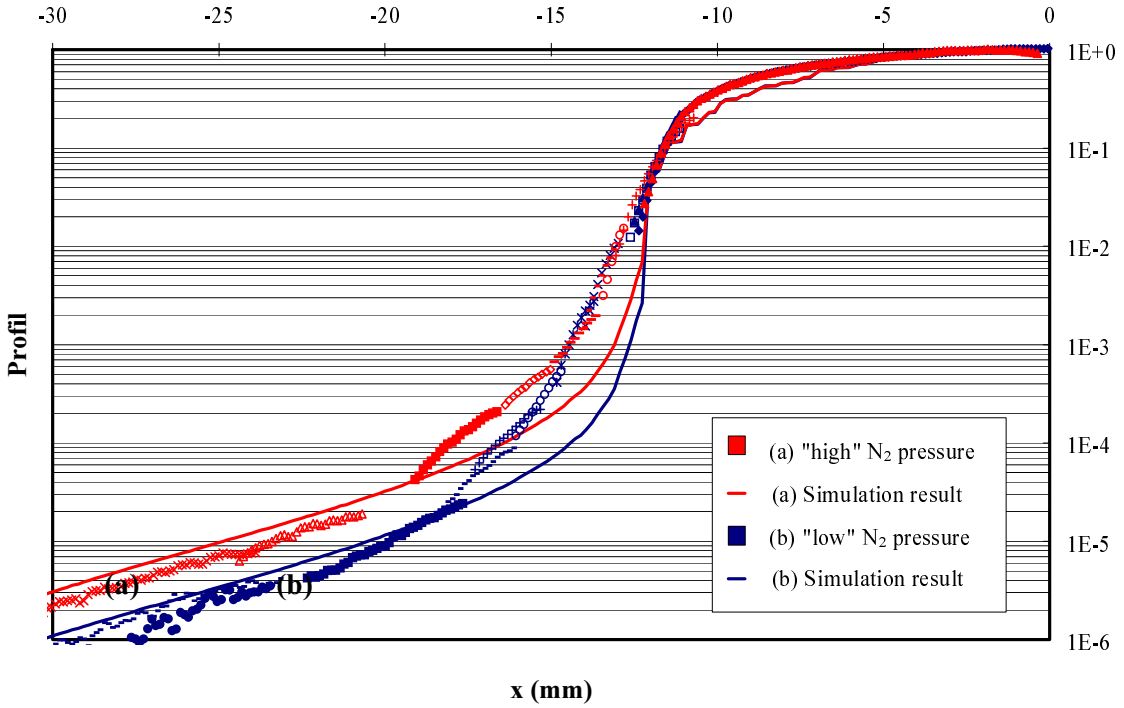

Fig. 5 : Experimental and simulated beam profile in two different nitrogen gas pressures.

	Begining	**Middle**	**End**
"Low" N_2 pressure (hPa)	$6.4\ 10^{-6}$	$2.0\ 10^{-5}$	$3.2\ 10^{-5}$
"High" N_2 pressure (hPa)	$8.5\ 10^{-6}$	$6.0\ 10^{-5}$	$1.1\ 10^{-4}$

Table2 : The two pressure sets in the experiment measured at the begining, the middle and the end of the drift space.

We observe that an increase of the residual gas pressure, by approximately a factor 3 in the second part of the drift space, induces an increase of the beam halo intensity by the same factor. Other measurements, not presented here, obtained for 8 different gas pressures exhibit the same behaviour but more precisely.

3.2. Simulation of the experiment

We have simulated the experiment using the analytical results presented in section 0. The simulation method is schematically presented in **Fig. 6** and described below :

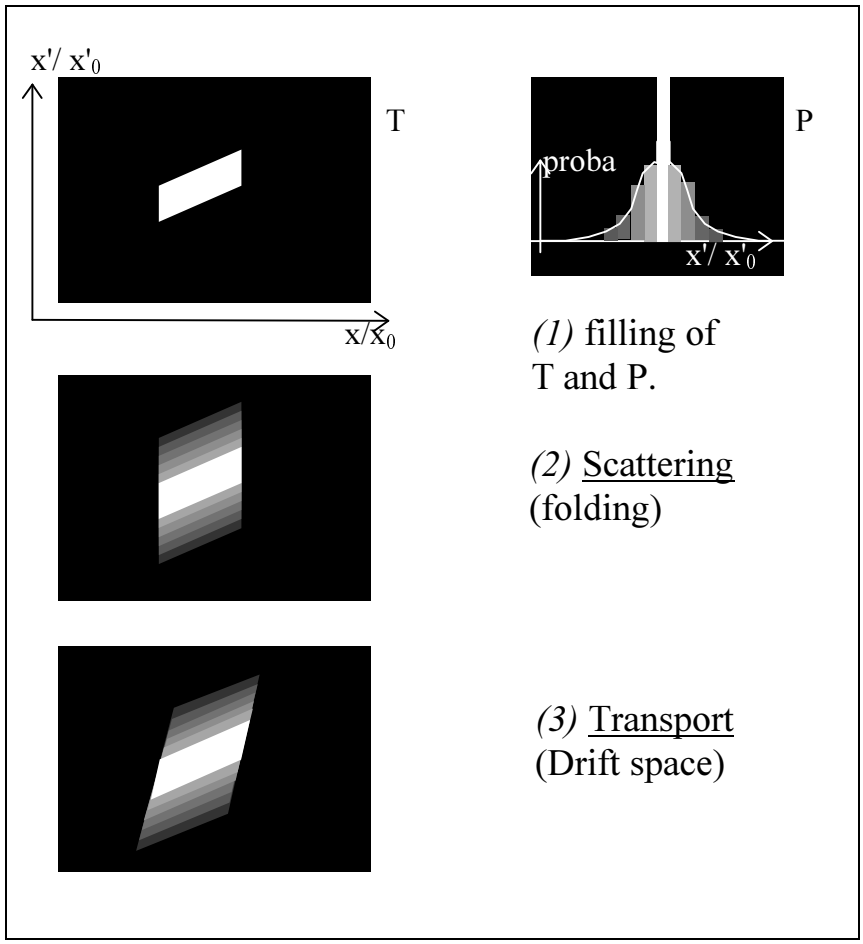

Fig. 6 : Schematics relevant to the simulations.
See text for explanations.

A 2D array (called T, with a size of N×M) contains the beam density distribution digitised in the (x,x') phase space. It is sampled with a step dx in the x direction and a step dx' in the x' direction. $T_{i,j}$ then represents the beam density for x between ((i+1)-N/2)dx and (i-N/2)dx and for x' between ((j+1)-M/2)dx' and (j-M/2)dx'. This array is initially filled with a homogeneous parallelepiped, corresponding approximately to the measurement of the beam distribution in this (x,x') phase space presented in ref. [4] (See **Fig. 6-*(1)***).

A 1D array (called P, with a 2M size) contains the probability for a particle to scatter at an angle θ_x between i.dx' and (i+1).dx', i being the index in the 1D array. We have $P_i=\{\text{Ꝑ}(\theta_x>[(i+1)-M].dx'_e)-\text{Ꝑ}(\theta_x>[i-M].dx'_e)\}dz$. The term Ꝑ() is calculated using formula **(10)**, dz is the longitudinal processing step length. We note that dx' is the numerical sampling step in both arrays T and P.

We then simulate the evolution of the beam distribution function. We choose, for that, a processing step length dz and for each step, we determine :

- The beam scattering, by folding each column of array T (at $x=C^{ste}$) with the array P (See **Fig. 6-*(2)***),

- The beam transport, by translating each point of the phase space pattern T along the x axis of a quantity proportional to the co-ordinate x' (that is $x_f=x_i+x'.dz$, $x'_f=x'_i$). This corresponds to the beam transport in a drift space without space charge effect (See **Fig. 6-*(3)***).

The difficulty of this study arises from the fact that the particles are scattered in the x' direction of the phase space, and that we want to observe the scattering effect in the x direction. The coupling between directions x and x' is obtained from the beam transport parameters.

We have assumed here that the scattering probability in the x' direction is independent of the initial slope x_i' of the particle trajectory. In fact, this is not really true, but in the case of small x_i' and small scattering angles, it is a good assumption to consider the scattering distribution as being the same as that of a zero divergence particle beam.

The space-charge effect on the beam-size growth is not taken into account in our simulation code. Thus, in order to compare precisely the experimental and simulation results, we have multiplied the x axis of the profile obtained from the simulation by a factor k which has been determined to obtain the same beam-core diameter for experiment and simulation (k=1.7 in this experiment). The simulation results are also shown in **Fig. 5**, they have been established for the pressure conditions of the experiment. However, pressure values at intermediate positions along the transport line have been determined by linear interpolation between the three measurements.

Although the space charge effect is roughly considered, the particle motions in the x and y directions are assumed to be independent, the detailed initial beam emittance and the exact gas-pressure distribution are not taken into account in our simulation code, the calculated results are in quite good agreement with the experimental data, especially far from the beam centre, beyond 1.5 times the beam-core radius. We observe, however, a discrepancy between the measured and simulated transverse distributions in the halo region close to the beam-core (between 1 to 1.5 times the beam-core radius). This can be explained by the crude description of the initial beam emittance in the simulation, which leads to sharper beam edges than for the experiment. This experimental "nearby" halo, whose shape seems to be independent of the gas pressure, may be, also, created by space charge effect within the beam. Nevertheless, we can conclude that our simple model of beam scattering on the residual gas is good enough to allow predictions on the scattering halo formation in the FODO experiment, or in a high intensity linear accelerator.

4. Simulation of the FODO experiment

We now consider the simulation of a proton beam transport in our FODO experiment [4]. To simplify the simulation, the beam is assumed to be transported in a uniform focusing channel of 10 meters in length. From the scattering point of view, it is nearly equivalent to the transport in a periodic focusing channel. Moreover, we assume that the proton beam has a Kapchinsky-Vladimirsky (K-V) distribution [9] in the transverse phase space, which means

that the emittance ellipse in the (x,x') phase space is homogeneous. In addition, we consider that the beam is matched in the channel. This means that, in the K-V conditions, each beam particle moves in a harmonic-oscillator potential well. The other beam properties are: a proton beam energy of 500 keV, a maximum angular spread $x'_0=\pm 2$ mrad, a residual gas of monoatomic oxygen (Z=8) and a betatron wavelength of 4 m. The transverse beam size is a parameter which does not influence the simulation results.

The simulation method is nearly the same as that used for the drift space and described above. The only differences are the following :

- The array T is initially filled with a homogeneous disc, corresponding to the projection of the beam K-V distribution in the transverse phase space.

- We choose a processing step length, dz, much smaller than the betatron oscillation wavelength.

- The beam transport, for each step dz, consists in rotating the phase space pattern T of an angle $\theta = 2\pi \frac{dz}{Z}$. This corresponds to the beam transport in a harmonic oscillator potential well.

The beam profile obtained at the exit of the channel is represented in **Fig. 7**, for different pressure values. We can notice that the collisional halo develops very far away from the core.

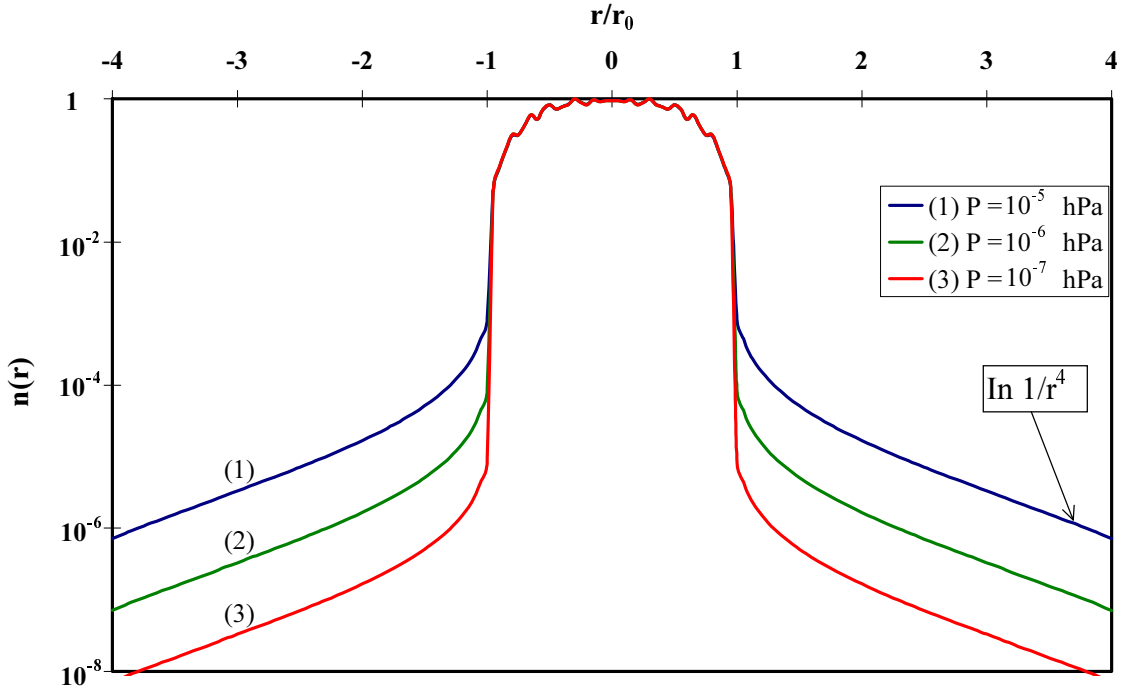

Fig. 7 : Influence of the scattering process on the beam profile
The different curves correspond to different gas pressures.

5. Discussion about influence of space-charge

When the beam is space-charge driven, 2D phase-space beam distributions are no longer ellipses, but tend to rectangles. In that case, particle trajectories (iso-hamiltonian curves) are not ellipses in phase-space, but are curves whose shape depends on the beam distribution trough the space-charge potential.

When the beam is space-charge dominated, it can be assumed that iso-hamiltonian curves in (x/x_0, x'/x'_0) are nearly rectangles [10] (as represented in **Fig. 8**). In that case, in order to get the same amplitude, a particle need to be scattered to an angle larger than the one that would have been necessary with no space-charge force (where ellipses are the iso-hamiltonian curves).

This situation can be seen an other way: When there are space-charge forces, more external focusing forces are needed to transport the beam with the same size. In that case, the confinement potential well is deeper, and the kinetic energy (get by a collision) needed to get the same amplitude is higher. This will decrease the Residual gas scattering halo.

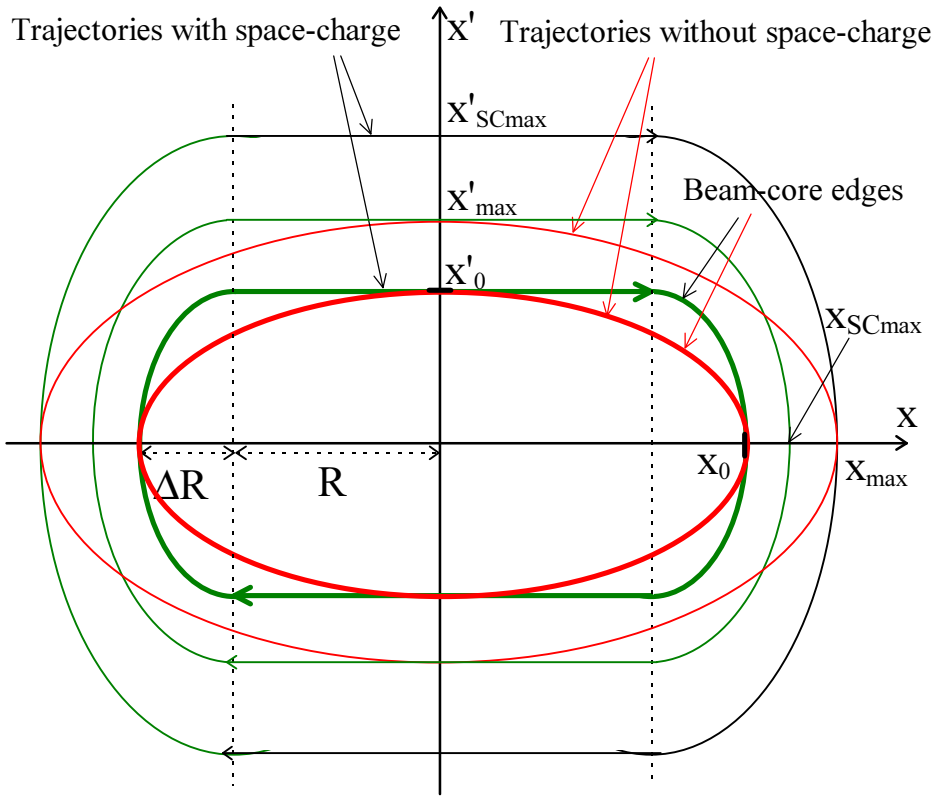

Fig. 8 : Beam shape and particle trajectories around a beam with :
- No space-charge forces (ellipses, in red),
- Space charge forces (quasi-rectangles, in green).

The scattering angle necessary to get an amplitude x_{max} is larger with space-charge than without space charge.

If k_0 is the external focusing phase advance per meter, and η is the depress-tune factor of the beam, then :

$$x'_0 = \eta\, k_0 \cdot x_0 ,$$

R is the homogenous-part beam size, and ΔR is its border size, then :

$$x_0 = R + \Delta R ,$$

If particles outside the beam feel only external forces, we can assumed[1] that :

$$\Delta R = \frac{x'_0}{k_0}, \text{ which gives } R = x_0 - \frac{x'_0}{k_0} = x_0 (1 - \eta).$$

Two particles scattering to the same angle x'_{max}, will not reach the same amplitude depending on whether we take into account space-charge (x_{SCmax}) or not (x_{max}). We have :

$$\frac{x_{SC\,max}}{x_{max}} = \frac{R + x'_{max} / k_0}{x'_{max} / k_0} = \frac{R + \eta x_{max}}{x_{max}} = \eta + (1 - \eta) \cdot \frac{x_0}{x_{max}}.$$

The space charge decreases the particle amplitude by a factor between 1 (close to the core when $x_{max} = x_0$) to η (far from the core when $x_{max}/x_0 \to \infty$).

The amplitude density is increased because the scattering x-slope range for which particle have amplitude between x and x+dx is larger with space-charge than without space-charge. This amplification factor is : $\frac{d\, x_{SC\,max}}{d\, x_{max}} = \eta + (1 - \eta) \cdot \frac{x_0}{x_{max}}$.

Halo density calculated without space-charge is overestimated the one with space-charge effects. Curves presented on **Fig. 7** must be corrected (see **Fig. 9**) in order to take into account space-charge effects by making the transformations :

$$\begin{cases} n(x) = \dfrac{n(x)}{\left(\eta + (1 - \eta) \cdot \dfrac{x_0}{x}\right)} \\ x = x \cdot \left(\eta + (1 - \eta) \cdot \dfrac{x_0}{x}\right) \end{cases}.$$

[1] The logarithm contribution of the space-charge potential has been neglected.

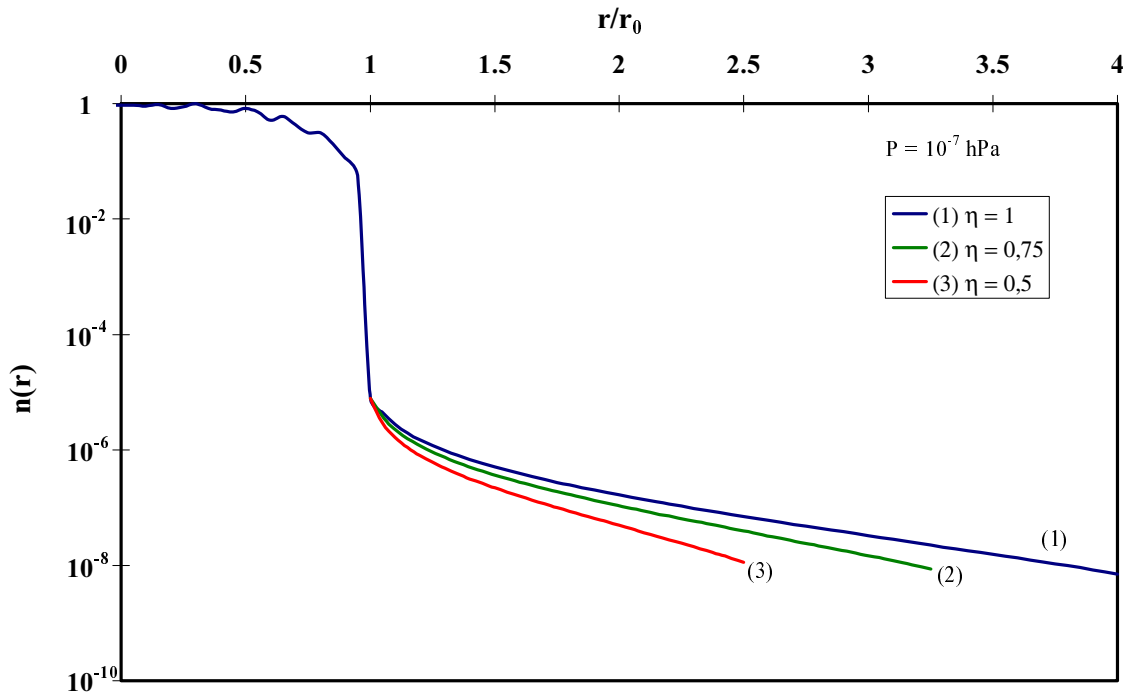

Fig. 9 : Space-charge influence on the particle amplitude distribution.

Due to the profile variation in $1/r^4$ far from the core, the beam far-halo density will be decreased by a factor η^3.

6. Beam losses in a high intensity TRISPAL linac

6.1 TRISPAL Linac

The proton TRISPAL linac [11] is composed of 4 different parts (**Fig. 10**) :

1- ECR source (SILHI, 100 keV, 40 mA (up to 100 mA) protons),

2- RFQ (from 100 keV to 5 MeV),

3- DTL-CCDTL (from 5 MeV to 100 MeV),

4- CCL (from 100 MeV to 700 MeV).

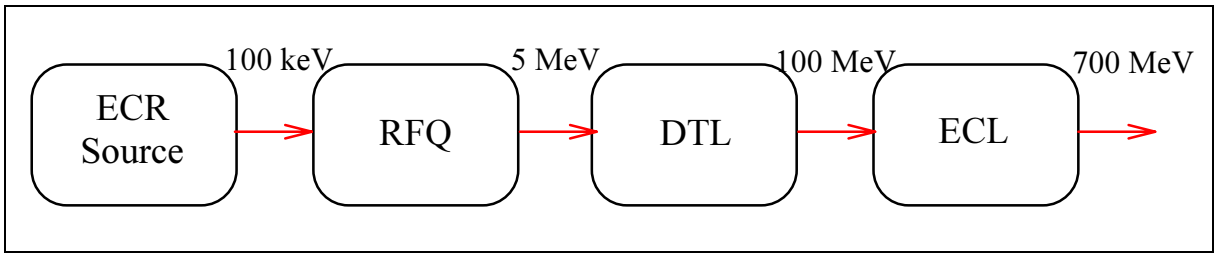

Fig. 10 : TRISPAL Linac

The residual gas in the linac will be responsible of halo formation.

Residual gas scattering is more important at low energy than at high energy, firstly because of the scattering cross section varying in (kinetic energy)$^{-2}$ and secondly because of the higher gas pressure close to the source.

Nevertheless, because the beam size and normalised emittance are kept constant along the acceleration, the beam angular spread decreases in 1/p (p being the particule momentum). In consequence, the scattering angle allowing to reach the halo decreases in 1/p.

In addition, as shown in **Table 1**, acceptable loss rate decreases with energy.

Energy (MeV)	10	20	50	100	200	500	1000
Acceptable losses (nA/m)	200	15	2,5	1	0,2	0,05	0,03

Table 1 : Proton losses inducing a 2.8 mrem/hr gamma dose at 1 m from the linac after 1 hour decay.

6.2 Basic model

Let's modelise the TRISPAL linac with a continuous focusing channel, increasing smoothly the matched beam energy from 10 MeV to 1 GeV. The beam RMS normalised emittance is constant along the transport : $\varepsilon_{nRMS} = 2{,}4\ 10^{-7}$ π.mm.mrad. The RMS beam size is kept constant too : $\sigma_x = 3$ mm. Linac pipe has a $\phi = 28$ mm diameter. Space-charge depress tune used in this model is $\eta = 1$ (no space-charge forces).

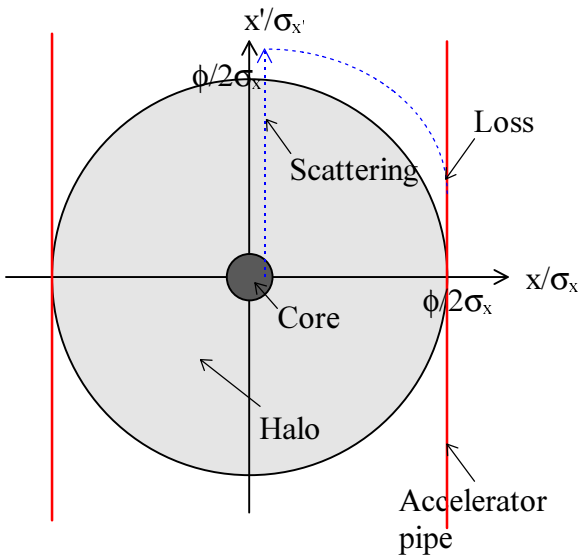

Fig. 11 : Particle scattering inducing loss

Particle trajectories in (x/σ_x, $x'/\sigma_{x'}$) phase-space are circles. σ_x is the rms-beam size in x direction and $\sigma_{x'}$ is the beam rms-slope spread in the same direction. A particle scattering to an angle $x' > x'_{max}$ will be directly lost (after ¼ of betatron period) if :

$$x'_{max} = \frac{\phi \sigma_{x'}}{2 \sigma_x}.$$

A particle which scatter to an angle x' > some $\sigma_{x'}$, will enter the halo.

On **Figure 12**, have been represented direct losses of a 100 mA beam. They are compared with acceptable losses given by **Table 1**. The Nitrogen (Z=7) residual gas pressure is 10^{-7} hPa.

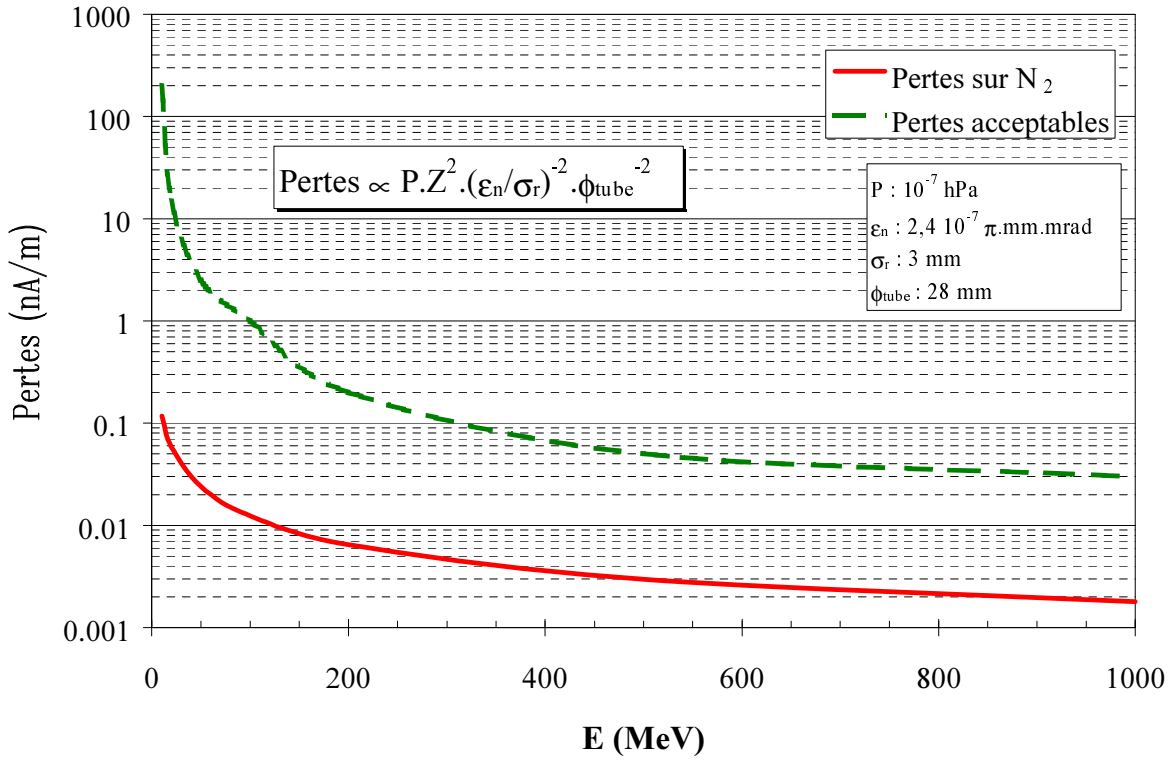

Fig. 12 : Direct losses in residual gas for TRISPAL linac

Remarks :

- As shown on **Fig. 12**, losses are proportional to the gas pressure, the square of charge number, and inversely proportional to the square of angular spread and of pipe diameter.

- Losses in hydrogen gas (Z=1), are 50 time lower than those in Nitrogen. In fact, partial pressure of all gas, and especially those of heavy gas as rare gas or hydrocarbon has to be taken into account.

- The gas pressure is not constant over the accelerator. Between vacuum pumps, the gas pressure can be several time the one at pump position.

- The use of all "with gas" element will induce localised losses.

6.3 Extension of the basic model

In the basic model, some assumptions have been done. Let's have a look on their influence.

6.3.1 Space-charge influence

With space-charge ($\eta<1$), as seen previously, scattered particles don't have the same phase advance per meter than those of the core. This increases the maximum angle beyond which the particle is lost. Direct losses are then reduced by a factor $1/\eta^2$.

6.3.2 Periodic transport

In a real linac, the transport channel is not continuous but periodic. The beam size is then oscillating around a mean value, and get higher value in focusing quadrupoles. In the basic model, continuous losses have been considered as they are actually localised in quadrupoles.

6.3.3 Non direct losses

On **Fig. 12** have been taken into account direct losses. But a lot of scattering particles are not lost but enter into the beam halo, and are potential losses (dangerous in case of mismatch and misalignement).

In TRISPLA linac, at 600 MeV, beam fraction intensity stored from the energy of 10 MeV, with a mean acceleration of 1 MeV/m, in a 10^{-7} hPa Nitrogen gas pressure, between 25 mm and 28 mm (close to the pipe) is 1,4 nA, then 30 times acceptable losses per meter at this energy !!

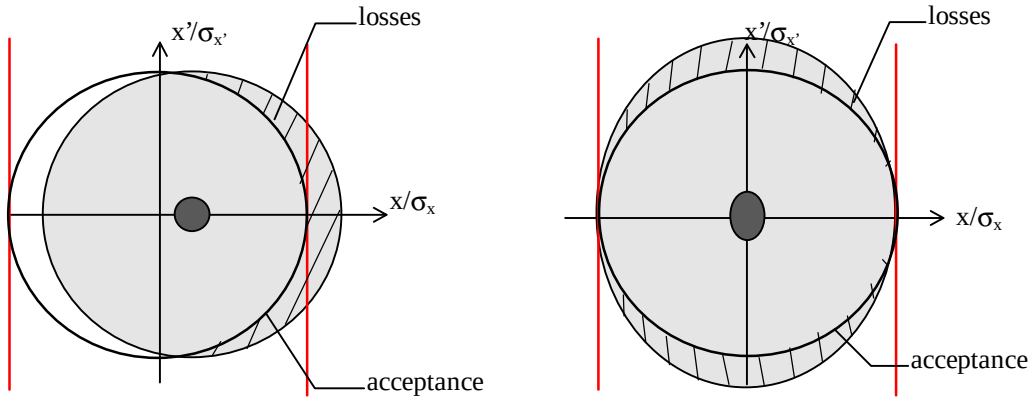

Of centered beam Mismatched beam

Fig. 13 : Basic representation of the effect of some transport errors on beam losses.

In case of misalignement and mismatch, or a change of accelerator acceptance (for example in matching sections), the beam will undergo localised losses.

7. Conclusions

In the conditions of our planned FODO experiment, the scattering process of the beam particles on the residual gas in the evacuated transport line will strongly compete with other halo-producing phenomena such as the particle-core coupling through transport dynamics.

In a linear accelerator, the scattering process can be very significant, particularly in the low-energy end and near the source, where the vacuum pressure is generally high. The transport of this "collisional halo" through the high-energy sections, where its effects may be serious has to be studied. A mean of eliminating it before it reaches these sections has to be found.

We notice that the more the angular spread of the beam is, the less important the scattering effects are. This means that, for a given emittance, it is better to transport a small-size beam, with large angular spread. This goes in the way of decreasing the tune depress η.

Losses can be reduced :

- By decreasing the residual gas pressure and particularly this of heavy gas (losses $\propto P \cdot Z^2$),

- by using strong focusing forces (losses $\propto \sigma_x^2 \cdot \eta^2$),

- by increasing the pipe diameter (losses $\propto \phi^{-2}$), even if this is not very efficient for this kind of losses.

- by watching carefully the beam matching and misalignement. The acceptance should not decrease in order to avoid localised losses.

As a consequence of the huge diffusion at low energy, it seems interesting to clean the beam at low and medium energies.

8. References

[1] J.M. Lagniel, *Chaotic behaviour induced by space-charge*, EPAC 94, London, Great Britain, 27 June - 1 July 1994, Conf. Proc. vol. 2, p.1177.

[2] C. Chen and R.A. Jameson, *Self-consistent simulation studies of periodically focused intense charged-particle beams*, Phys. Rev. E**52** (1995) 3074.

[3] M. Reiser, *Theory and design of charged particle beams*, J. Wiley & Sons, Editor, p.539.

[4] P-Y Beauvais et al., *Studies on halo formation in a long magnetic quadrupole FODO channel - First experimental results*, PAC 95, Dallas, Texas, USA, 1-5 May 1995.

[5] J.M. Lagniel, *Chaotic behavior and halo formation from 2D space-charge dominated beams*, Nucl. Instr. and Meth. A**345** (1994) 405.

[6] H. Straub, H. Bethe, J.Ashkin, N.F. Ramsey and K.T. Bainbridge, *Experimental nuclear physics*, Vol. 1, E. Segre, Editor, p.251.

[7] J.D. Jackson, *Classical Electrodynamics*, second edition, J. Wiley & Sons, Editor, p.650.

[8] N. Pichoff, G. Haouat et al., *Experimental study of the ELSA electron-beam halo*, 2nd European Workshop on Beam Diagnostics and Instrumentation for Particle Accelerators, Travemünde, Germany, 28-31 May 1995, Conf. Proc. p.63.

[9] I. M. Kapchinsky and V. V. Vladimirsky, *Proc. International Conf. on High Energy Accelerators*, CERN, Geneva, 1959, p.274 ff.

[10] N. Pichoff et al., *Stationary distribution of space-charge driven continuous beam*, Note DAPNIA/SEA 98/43.

[11] J.M. Lagniel, *High Intensity Linac Study in France*, LINAC 98, Chicago, August 23-28, 1998.